PHYSICAL REVIEW E **91**, 011002(R) (2015)

Bridging the gap between an isolated nanochannel and a communicating multipore heterogeneous membrane

Yoav Green, Sinwook Park, and Gilad Yossifon*

Faculty of Mechanical Engineering, Micro- and Nanofluidics Laboratory, Technion–Israel Institute of Technology, Technion City 32000, Israel

(Received 1 September 2014; revised manuscript received 2 December 2014; published 28 January 2015)

To bridge the gap between single and isolated pore systems to multipore systems, such as membranes and electrodes, we studied an array of nanochannels with varying interchannel spacing that controlled the degree of channel communication. Instead of treating them as individual channels connected in parallel or an assembly like a homogeneous membrane, this study resolves the pore-pore interaction. We found that increased channel isolation leads to current intensification, whereas at high voltages electroconvective effects control the degree of communication via suppression of the diffusion layer growth.

DOI: 10.1103/PhysRevE.91.011002 PACS number(s): 47.57.jd, 47.61.Fg, 66.10.Ed, 82.39.Wj

Understanding ion transport processes through a heterogeneous permselective medium (membranes and nanoslots) is of great importance in realizing optimal designs of desalination, bimolecular sensors, and fuel cell devices [1,2]. In such systems, under the application of an external electric field, the ion-permselectivity symmetry breaking phenomenon results in ionic concentration polarization (CP), i.e., the formation of ionic concentration gradients. In this work we shall elucidate on the effect of the geometric heterogeneity and field-focusing effect in a nanoslot array on the CP and its associated diffusion-limited current. Thus far, nanochannel array systems that were previously investigated [3–5] treated the collective behavior as the sum of single and isolated nanochannels in the Ohmic regime. In this work, we shall show that neighboring channels interact such that the collective behavior also includes communication effects that are geometry dependent for all voltages. Understanding these effects in single and multiple channels or pores is of much importance to a wide variety of multipore structures, e.g., fabricated nanochannel array [3–5], membranes [6], and hierarchically micro- and nanoporous electrodes [7]. The fabricated nanoslot array serves as a simple and tractable model of the more geometrically complex ion-permselective membrane systems, thus allowing us to study the role of heterogeneity.

It is well established [8,9] that the current-voltage curve (I-V) of permselective systems exhibits three regimes: Ohmic, limiting-current, and over-limiting-current (OLC). In the low-voltage (i.e., under-limiting) regime, the current increases linearly with the applied voltage, in conjunction with ionic depletion at the micro-nanochannel interface through which the counterions are entering. Theoretically, under the assumption of local electroneutrality (LEN), the system cannot sustain currents larger than a limiting value [8] corresponding to the complete depletion of the salt concentration at the microchannel-permselective medium interface. In practice, measurements showed that currents could surpass this theoretically predicted value. An early work [9] showed that by waiving the LEN assumption, an extended space charge layer (SCL) is formed at the entrance of the permselective interface, resulting in large yet finite differential resistance within the limiting-current regime. Other possible mechanisms responsible for the increase of the conductivity in this regime are related to the charged microchannel walls through surface conductance [10], electro-osmotic flow (EOF) [11,12], Taylor dispersion [13], and also surface charge regulation [14].

Two electroconvective (EC) mechanisms associated with the emergence of the SCL that have been shown to be responsible for the OLC are Dukhin's EOF of the second kind [15] and Rubinstein and Zaltzman's electro-osmotic instability (EOI) [16,17]. In both mechanisms it is the tangential component of the electric field that acts on the SCL to form an electric body force that drives the vortex pairs. However, the former is commonly associated with geometrically heterogeneous systems wherein a tangential field always exists. In contrast, the latter is associated with homogeneous systems wherein the tangential component of the field is vanishingly small, thus, resulting in quiescent flow conditions. Rubinstein and Zaltzman [16,17] showed that beyond a critical voltage the SCL loses its stability and forms an array of EC vortices.

The formation of these vortices suppresses the otherwise unbounded diffusive growth of the depletion region, which in turn results in a shorter selected diffusion layer (DL) length that is responsible for the transition to OLC. These have been observed in a number of recent experiments for wide nanoslot [18], homogeneous membrane [19], and a heterogeneous array of narrow nanoslots [3,4]. The interplay between these two EC mechanisms has recently been studied numerically for a geometrically modulated membrane surface [20] and observed experimentally for a wide nanoslot [21]. However, here we focus on the effect of geometric heterogeneity of the nanoslot interface on the ion transport in the Ohmic, limiting-current, and OLC regimes.

A number of recent theoretical works have studied the effects of geometric heterogeneity in permselective systems undergoing CP in two dimensions [22,23] and three dimensions [24,25], however, these effects have not been verified directly in experiment. These theoretical works focused on CP under the LEN assumption and thus neglected the effects of both the SCL and EC. It was shown that both the geometries of the microchambers and the permselective medium determined the Ohmic and limiting responses. In particular, these theoretical descriptions apply to the case of an array of nanoslots or permselective medium which allows us to study the effect of interchannel spacing on the cumulative response

*Corresponding author: yossifon@tx.technion.ac.il

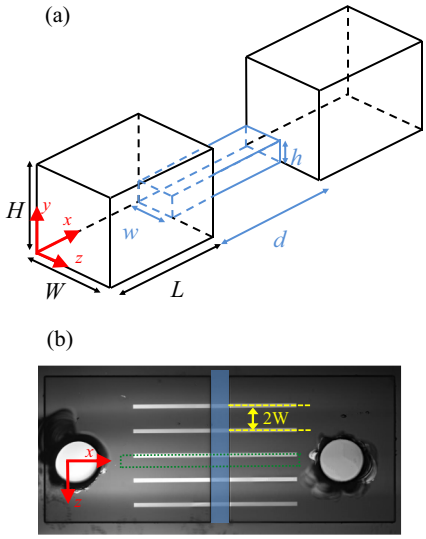

FIG. 1. (Color online) (a) Schematics describing half of a three-dimensional periodic unit cell consisting of a straight permselective medium connecting two opposite symmetric microchambers. (b) An optical top-view (x-z plane) image of a nanoslot array (half unit cell is marked by a dotted green box, while the yellow dashed lines mark the distance between the center of two adjoining channels, $2W$). The microchamber has a height of $H = 48$ μm and a width of $\sim$3 mm. The approximate distance of the drilled holes from the permselective interface is $L \sim 2$ mm. The nanoslots have a width of $2w = 92$ μm, height $h = 178$ nm, and length $d = 0.35$ mm. The number of channels and their spacing varies as given in Table I. Note the depiction in (a) is not to scale.

of the array. This is the embodiment of the interchannel communication in the Ohmic and limiting regimes, where electrodiffusion effects, with negligible electroconvection, are sufficient for its description. Here we shall experimentally substantiate these theoretical predictions regarding the effect of geometric heterogeneity, in the form of a nanoslot array with varying interchannel spacing, on the CP, and in turn, on the diffusion-limited current. Furthermore, our experimental results extend also into the OLC regime where EC effects become significant and result in a complex response which currently lacks theoretical grounds. Hence, in contrast to the more predictable response in the Ohmic and limiting regimes, the interchannel communication in the OLC regime will be described in a more qualitative manner.

The microfabricated device consists of an array of identical nanoslots of varying interchannel spacing (see Fig. 1, Table I, and Fig. S1 in [26]) flanked between rectangular microchambers. Details on the fabrication process and the measurement technique are found in the Supplemental Material [26].

TABLE I. Half periodic unit cell width, W; total number of array channels, N; and geometric ratios as given by Eq. (1).

Nanoslot array name	W (μm)	N	$\frac{L}{HW}(\frac{10^5}{m})$	$\frac{\bar{f}}{L}(\frac{10^4}{m})$
Array A	$\sim$1500	1	0.28	6.00
Array B	285	5	1.46	4.87
Array C	200	7	2.08	4.65
Array D	165	7	2.52	4.51
Array E	93	7	4.48	4.15
Array F	93	13	4.48	4.15

After cleaning the channels [26], a KCl solution of low concentration, 30 μM, was introduced to ensure electric double layer (EDL) overlap (Debye length of $\lambda_D \approx 55$ nm) [27]. For each configuration (Table I) $\sim$7–8 I-V sweeps were conducted between 0 and 50 V at increments of 0.25 V and a time step of 10 s. The mean value and standard deviation of these measurements are calculated for each channel separately (Fig. S2 of [26]). Figure 2(a) depicts the measured mean current for each nanoslot array configuration. Expectedly, the current increases with an increasing number of channels as the total Ohmic resistance of the nanoslot array (not including the microchambers and field-focusing resistances [25]) decreases according to $R_{\text{array}} = R_{\text{unit cell}}/N$, where $R_{\text{unit cell}}$ is the resistance of the periodic unit cell (Fig. 1), as these are connected in parallel.

Previous works have focused on microchamber-nanochannel systems with dominating nanoslot resistance [5,27,28]. In a more recent work, a model system similar to our experimental setup, comprising a periodic array of nanoslots, was studied theoretically [25] for the case of comparable microchannel and nanochannel resistances. In contrast to a recent paper [29] in which the ionic transport through an array of nanopores was studied under conditions of vanishing permselectivity, the former study [25] and this current work account for the nanoslots ionic permselectivity and the resulting CP. It was shown [25] that the total Ohmic conductance of an ideal permselective system was comprised of three components according to the system geometry (Fig. 1): nanochannel resistor (first term), microchamber resistor (second term), and geometric field-focusing resistor (third term):

$$\sigma = \frac{\hat{I}}{V} = \frac{I/N}{V} = 2\frac{DF^2c_0}{RT}\left(\frac{d}{hw\Sigma} + \frac{2L}{HW} + 4\frac{\bar{f}}{L}\right)^{-1}, \qquad (1)$$

where D is the ionic diffusion coefficient, R is the universal gas constant, T is the absolute temperature, and F is the Faraday constant. Herein, $\Sigma = \tilde{\Sigma}/c_0$ is the excess counterion concentration (normalized by the bulk concentration c_0) exactly compensating the (negative) surface charge within the nanoslot and $\bar{f} = \bar{f}(L,H,h,W,w)$ is a geometric nondimensional function with a strong dependence on the two heterogeneity parameters h/H and w/W (the full form of the $\bar{f}$ function can be found in Eq. (26) of Ref. [25]). In the current contribution, the former ratio has been kept constant and the latter has been varied. In addition, it was shown that $\bar{f}$ is a monotonically increasing function of decreasing w/W and equals zero when the system is homogeneous ($w = W$ and $h = H$). Hence, the microchamber (second term) and the field-focusing (third term) resistors in Eq. (1) counteract each other with the change of the system geometric heterogeneity (i.e., W/w, while keeping w constant), with the former decreasing with increasing W/w and vice versa for the latter (Table I).

In the case of nanochannel dominated resistance one would expect that the current per channel versus voltage curves should collapse onto each other. Figures 2(b) and 2(c) depict the current per channel (i.e., $\hat{I} = I/N$) for the voltage range of 0–50 V and 0–15 V, respectively. It is clearly

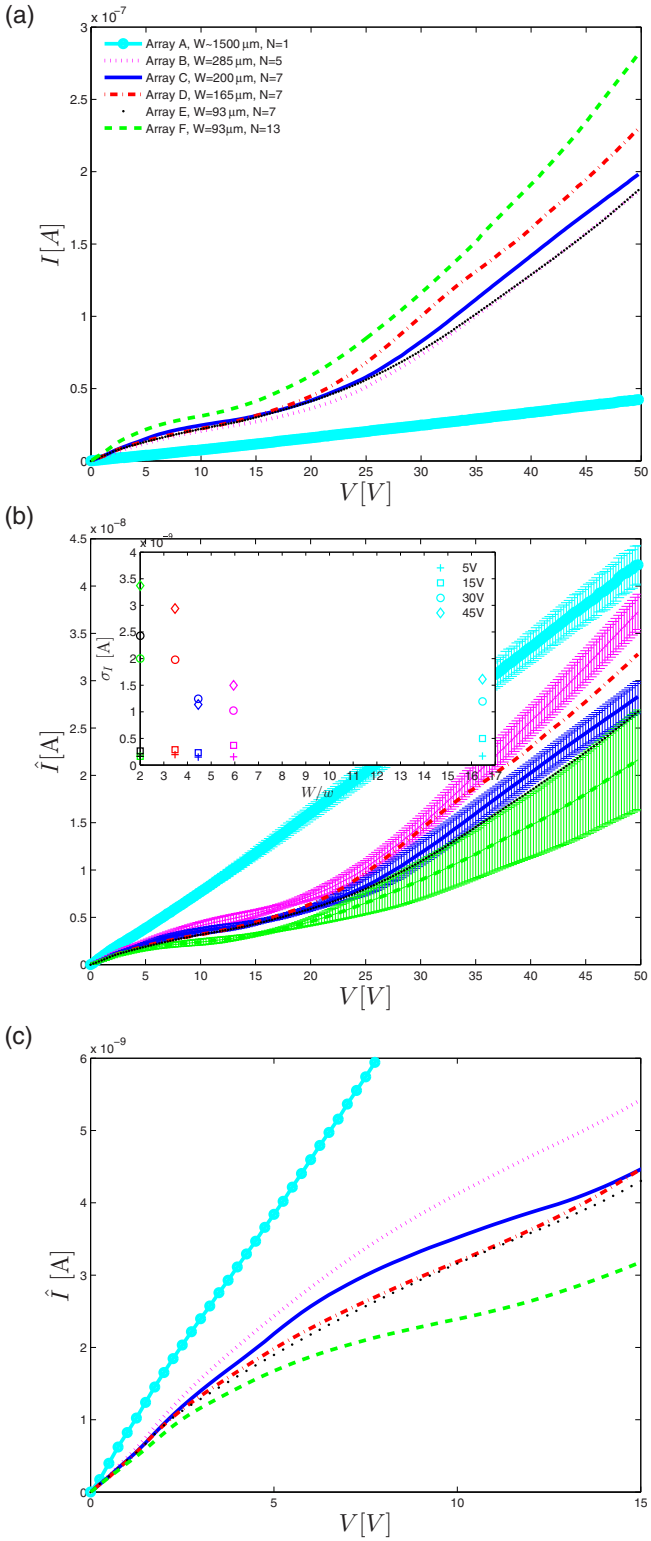

FIG. 2. (Color online) I-V curves for channels of varying interchannel spacing depicting (a) the total average current, I; and (b) the average current per channel, $\hat{I} \equiv I/N$. For clarity purposes a single standard deviation, σ_I, is demonstrated only for arrays A, B, C, and F. The inset shows the calculated standard deviation at various applied voltages as a function of the periodic unit cell half-width, W, normalized by the nanoslot half-width, w. The color scheme follows that of the legend given in (a). (c) A close-up of the Ohmic and limiting current regimes of (b).

seen that the conductance (i.e., slope of the I-V curves) per channel is not identical but rather depends on the interchannel spacing (specifically, increasing with increasing W). This is a consequence of the fact that the combined contribution of the microchannel and geometric field-focusing resistances in our device are comparable to that of the nanochannel. The first term in Eq. (1) can be evaluated based on the range of values $\Sigma = \tilde{\Sigma}/c_0 = [(-2\sigma_s/h)/F]/c_0 \approx 27-233$ (wherein σ_s is the surface charge density and was evaluated as $\sigma_s = -7 \times 10^{-3}$ C/m^2 in Ref. [28] and $\sigma_s \approx -6 \times 10^{-2}$ C/m^2 in Refs. [5,27]) yielding $d/hw\Sigma = 1.8 \times 10^5 - 1.6 \times 10^6$. The calculated resistance of an array of nanoslots is simply $R_{\text{array}} = R_{\text{unit cell}}/N = (\sigma N)^{-1}$, which, for example, in the case of a single nanoslot ($N = 1$) yields $R_{\text{array}}|_{N=1} \sim 1-4.2$ GΩ. This is consistent with the experimentally measured value based on the slope in the Ohmic region $R_{\text{array}}|_{N=1} \sim 1.2$ GΩ. Another consequence of heterogeneity is the limiting-current dependence on the microchamber geometry [24,25]

$$\hat{I}_{\text{lim}} = 2DFc_0\left(\frac{L}{2HW} + \frac{\bar{f}}{L}\right)^{-1} \tag{2}$$

which is evident in Fig. 2(c).

We confirm these predictions in the following manner. Three arrays with the same number of nanoslots but varying interchannel spacing (arrays C, D, and E) were measured and are compared with the single channel (array A). As predicted from Eq. (1), the Ohmic conductance decreases with decreasing heterogeneity (i.e., decreasing W/w) such that $\sigma_A > \sigma_C > \sigma_D > \sigma_E$. An additional test group is arrays B, C, and F whose total *active* array width, $\sim 2WN$, is approximately the same. Array F, which is comprised of the largest number of nanoslots, expectedly, exhibits the highest total current, yet, due to its relatively small heterogeneity (i.e., small W/w resulting in a small field-focusing resistor but large microchamber resistor), it has the lowest conductance and limiting current per channel [Fig. 2(c)]. Following array A (single channel), array B, which is the most isolated (multiple) channel, has the highest current per channel. The differences between arrays B, C, and F become even more pronounced when the current shifts from the Ohmic to the limiting regime when the microchamber geometry at the depleted side becomes increasingly important. Additionally the average current density per channel $\hat{I}/W$ exhibits (Fig. S3 of [26]) the expected reversal relative to the average current $\hat{I}$ [24].

The limiting currents of all channels as a function of geometric heterogeneity (W/w), excluding the single channel, are compared in Fig. 3 (see Supplemental Material to see how I_{lim} is defined [26]). We attribute the fact that the single channel case does not exhibit a limiting-current voltage window due to its strong isolation that results in a large tangential electric field which drives a single pair of electro-osmotic (EO) vortices of the second kind (Dukhin mechanism [15]). The more efficiently mixed depleted region eliminates the saturation of the diffusion-limited current, which is in agreement to a previous study of varying nanoslot width [28]. We approximate the value of the limiting current to be that corresponding to a minimal differential conductance (Fig. S2 [26]). To facilitate comparison between measured and theoretically predicted

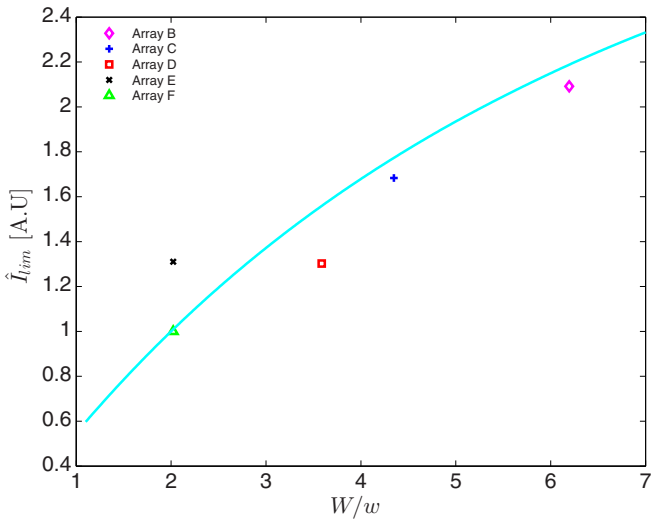

FIG. 3. (Color online) Limiting currents (per channel) normalized by that of array F versus system heterogeneity, W/w. Symbols represent experimental data; the continuous line represents the theoretical model [Eq. (2)].

limiting currents [Eq. (2)] we normalize both to that of array F (Table I), yielding fair agreement between theory and experiments. We note a peculiarity with the limiting current of array E—it is larger than that of array F, although both have the same interchannel spacing. This is probably due to the fact that array E's fewer nanoslots ($N = 7$) are located at the center of the device whereas in array F the nanoslots ($N = 13$) are less centralized, thus, their effective distance from the reservoir (see Fig. 1) is larger, which in turn, results in a smaller limiting current.

We finally wish to address the effects of EC. In the Ohmic and limiting-current regimes the effects of EC are small, regardless of the heterogeneity (w/W), as is evident by the small noise (standard deviation) measured for all arrays [inset of Fig. 2(b) and Supplemental Material for the remaining standard deviations not given in Fig. 2(b)]. Since the EC effects are nonlinearly dependent on the applied voltage, these become the dominating mechanism for controlling the current at the OLC regime (see Supplemental Material [26] for movies demonstrating strong convection effects). Accordingly, the noise is monotonically increasing with increased voltage [inset of Fig. 2(b)]. Figure 4 shows the time evolution of array F under an applied voltage of 45 V and also the images of arrays A, B, and F after 200 s. In the OLC regime [inset of Fig. 2(b)] we can clearly see that the measured standard deviations get smaller with increasing channel isolation (i.e., high heterogeneity) and vice versa. An isolated channel has a distinct single vortex pair whose size is smaller than the interchannel spacing, which in turn, suppresses the diffusive growth of the depletion layer resulting in a smaller selected diffusion layer length (movies 1 and 2 [26]) and significantly

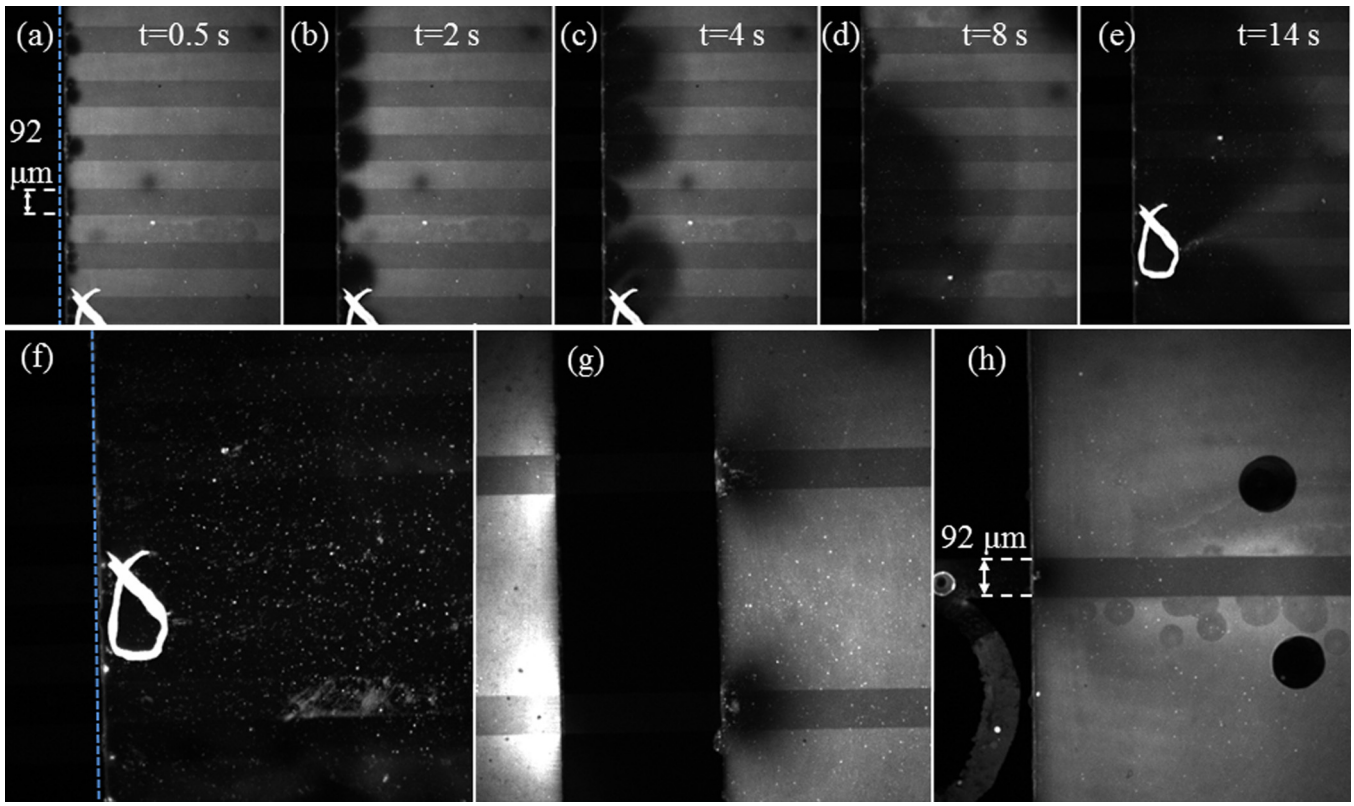

FIG. 4. (Color online) (a)–(e) Time evolution of the depletion and vortex array of array F under an applied voltage of 45 V. (f) At steady state, the depleted region eventually reaches the reservoirs. In contrast, for larger interchannel spacing, electroconvection slows down the diffusive growth of the depletion layer as seen in (g) for the most isolated (multiple) channels (array B) after 200 s (eventually the depletion regions merge) and in (h) for the single channel (array A) at steady state. The dashed blue line marks the interface of the nanochannel and microchambers.

lowers noise in the current. In contrast, at small interchannel spacing, smaller than the size of single vortex pair (movies 1 and 3 [26]), strong interchannel communication leads to electroconvection effects, reminiscent of the complex vortex and depletion array wavelength selection process due to the Rubinstein-Zaltzman instability [16,17]. It is likely that this complex and highly nonlinear coupled electrodiffusion and convection process increases the measured noise (standard deviation). In recent theoretical studies [30–32] it was even shown for homogeneous systems that interaction of the EC instability induced vortices leads to a chaotic behavior. Hence, the standard deviation results provide evidence of a competition [20,21] between the various EC modes, i.e., Dukhin's EOF of the second kind vs Rubinstein's EOI, in this array configuration.

In this work we have confirmed experimentally that geometric heterogeneity (through varying interchannel spacing) of a micro-nanochannel system undergoing CP not only changes the Ohmic conductance and the limiting current of the system, as was recently theoretically predicted [24,25], but also significantly changes its overlimiting response. Hence, proving interchannel communication effects to occur within all three regimes (i.e., Ohmic, limiting resistance, and OLC) of the current-voltage response. Specifically, both the conductance and limiting current per channel increase with increasing system heterogeneity. In addition, the OLC current is also highly dependent on the geometric heterogeneity where the EC vortices can either totally suppress the diffusive growth of the depletion layer (isolated channels) or contribute to a complex interchannel communication process eventually merging into a uniform diffusive front propagating all the way to the reservoirs. Moreover, the threshold voltage for the limiting to overlimiting current transition decreases with increased heterogeneity or channel isolation [Fig. 2(b)]. This also means that the limiting resistance voltage window vanishes with increased heterogeneity in agreement with previous studies [28,33]. However, further study with smaller interchannel spacing and channel width is required in order to test the validity of earlier predictions [28] that for a given active permselective surface there might be an optimal interchannel spacing that results in a local maxima of the OLC. Our findings, thus, serve as an initial step in understanding the full effects of geometrical heterogeneity on CP coupled with electroconvection on a breadth of communicating multipore structures, e.g., nanochannel array, membranes, and hierarchically micro-/nanoporous electrodes. It may also be useful for optimal design of pore spacing in synthesized membranes and fabricated nanochannel array.

This work was supported by Israel Science Foundation (ISF) Grant No. 1078/10. We thank the Technion RBNI (Russell Berrie Nanotechnology Institute) and the Technion GWRI (Grand Water Research Institute) for their financial support. Y.G. would like to thank the Rieger Foundation for their support.

[1] W. Sparreboom, A. van den Berg, and J. C. T. Eijkel, Nat. Nanotechnol. **4**, 713 (2009).
[2] R. B. Schoch, J. Han, and P. Renaud, Rev. Mod. Phys. **80**, 839 (2008).
[3] G. Yossifon, Y.-C. Chang, and H.-C. Chang, Phys. Rev. Lett. **103**, 154502 (2009).
[4] S. J. Kim, Y.-C. Wang, J. H. Lee, H. Jang, and J. Han, Phys. Rev. Lett. **99**, 044501 (2007).
[5] R. B. Schoch, H. van Lintel, and P. Renaud, Phys. Fluids **17**, 100604 (2005).
[6] V. I. Zabolotskii, V. V. Nikonenko, M. K. Urtenov, K. A. Lebedev, and V. V. Bugakov, Russ. J. Electrochem. **48**, 692 (2012).
[7] M. E. Suss, T. F. Baumann, M. A. Worsley, K. A. Rose, T. F. Jaramillo, M. Stadermann, and J. G. Santiago, J. Power Sources **241**, 266 (2013).
[8] V. G. Levich, *Physicochemical Hydrodynamics* (Prentice-Hall, New York, 1962).
[9] I. Rubinstein and L. Shtilman, J. Chem. Soc., Faraday Trans. 2 **75**, 231 (1979).
[10] A. Mani and M. Z. Bazant, Phys. Rev. E **84**, 061504 (2011).
[11] E. V. Dydek, B. Zaltzman, I. Rubinstein, D. S. Deng, A. Mani, and M. Z. Bazant, Phys. Rev. Lett. **107**, 118301 (2011).
[12] A. S. Khair, Phys. Fluids **23**, 072003 (2011).
[13] A. Yaroshchuk, E. Zholkovskiy, S. Pogodin, and V. Baulin, Langmuir **27**, 11710 (2011).
[14] M. B. Andersen, M. van Soestbergen, A. Mani, H. Bruus, P. M. Biesheuvel, and M. Z. Bazant, Phys. Rev. Lett. **109**, 108301 (2012).
[15] S. S. Dukhin, Adv. Colloid Interface Sci. **35**, 173 (1991).
[16] I. Rubinstein and B. Zaltzman, Phys. Rev. E **62**, 2238 (2000).
[17] B. Zaltzman and I. Rubinstein, J. Fluid Mech. **579**, 173 (2007).
[18] G. Yossifon and H.-C. Chang, Phys. Rev. Lett. **101**, 254501 (2008).
[19] S. M. Rubinstein, G. Manukyan, A. Staicu, I. Rubinstein, B. Zaltzman, R. G. H. Lammertink, F. Mugele, and M. Wessling, Phys. Rev. Lett. **101**, 236101 (2008).
[20] H.-C. Chang, E. A. Demekhin, and V. S. Shelistov, Phys. Rev. E **86**, 046319 (2012).
[21] Y. Green and G. Yossifon, Phys. Rev. E **87**, 033005 (2013).
[22] I. Rubinstein, Phys. Fluids A **3**, 2301 (1991).
[23] R. abu-Rjal, V. Chinaryan, M. Z. Bazant, I. Rubinstein, and B. Zaltzman, Phys. Rev. E **89**, 012302 (2014).
[24] Y. Green and G. Yossifon, Phys. Rev. E **89**, 013024 (2014).
[25] Y. Green, S. Shloush, and G. Yossifon, Phys. Rev. E **89**, 043015 (2014).
[26] See Supplemental Material at http://link.aps.org/supplemental/10.1103/PhysRevE.91.011002 for supplementary information and videos.
[27] D. Stein, M. Kruithof, and C. Dekker, Phys. Rev. Lett. **93**, 035901 (2004).

[28] G. Yossifon, P. Mushenheim, Y.-C. Chang, and H.-C. Chang, Phys. Rev. E **81**, 046301 (2010).

[29] A. Gadaleta, C. Sempere, S. Gravelle, A. Siria, R. Fulcrand, C. Ybert, and L. Bocquet, Phys. Fluids **26**, 012005 (2014).

[30] C. L. Druzgalski, M. B. Andersen, and A. Mani, Phys. Fluids **25**, 110804 (2013).

[31] E. A. Demekhin, N. V. Nikitin, and V. S. Shelistov, Phys. Fluids **25**, 122001 (2013).

[32] E. A. Demekhin, N. V. Nikitin, and V. S. Shelistov, Phys. Rev. E **90**, 013031 (2014).

[33] J. Balster, M. H. Yildirim, D. F. Stamatialis, R. Ibanez, R. G. H. Lammertink, V. Jordan, and M. Wessling, J. Phys. Chem. B **111**, 2152 (2007).